

JAAS

Accepted Manuscript



This is an *Accepted Manuscript*, which has been through the Royal Society of Chemistry peer review process and has been accepted for publication.

Accepted Manuscripts are published online shortly after acceptance, before technical editing, formatting and proof reading. Using this free service, authors can make their results available to the community, in citable form, before we publish the edited article. We will replace this *Accepted Manuscript* with the edited and formatted *Advance Article* as soon as it is available.

You can find more information about *Accepted Manuscripts* in the [Information for Authors](#).

Please note that technical editing may introduce minor changes to the text and/or graphics, which may alter content. The journal's standard [Terms & Conditions](#) and the [Ethical guidelines](#) still apply. In no event shall the Royal Society of Chemistry be held responsible for any errors or omissions in this *Accepted Manuscript* or any consequences arising from the use of any information it contains.

1
2
3 1
4
5
6 2
7
8
9 3 **UV light microscope: Improvements in optical imaging for a**
10
11
12 4 **Secondary Ion Mass Spectrometer**
13
14
15 5
16
17 6
18
19
20 7
21

22 8 Noriko T. Kita, Peter E. Sobol,
23

24 9 James R. Kern, Neal E. Lord, and John W. Valley
25
26
27
28 10
29
30 11
31

32 12 WiscSIMS, Department of Geoscience, University of Wisconsin-Madison,
33

34 13 1215 W. Dayton St., Madison WI 53706, USA.
35
36
37 14
38
39 15
40
41
42 16
43
44 17
45
46
47 18
48
49 19
50
51
52
53
54
55
56
57
58
59
60

Revised Manuscript January 30, 2015

submitted to

Journal of Analytical Atomic Spectrometry (JAAS)

1
2
3
4 20 Abstract: A large radius secondary ion mass spectrometer (SIMS) has been used for in-situ stable
5
6 21 isotope analyses of geological samples at the scale of 1-10 μm . However, the original reflected
7
8 22 light microscope of the CAMECA IMS 1280 SIMS had an optical resolution of $\sim 3.5 \mu\text{m}$, which
9
10 23 made it difficult to accurately position the analytical beam on the sample at the μm scale. We
11
12 24 modified the optical microscope to use ultraviolet (UV) light illumination and UV compatible
13
14 25 optical components, keeping the same mechanical design inside the vacuum chamber. The
15
16 26 optical resolution was improved to $1.3 \mu\text{m}$ with the UV-light optical system. In addition, we
17
18 27 wrote Badgerscope[©], a LabVIEW based software for sample imaging, which greatly enhanced
19
20 28 the accuracy of positioning and efficiency of instrument operation. These improvements can be
21
22 29 adapted to other micro-beam instruments where complex optical paths may be imposed by
23
24 30 instrument design.
25
26
27
28
29
30
31
32
33
34
35
36
37
38
39
40
41
42
43
44
45
46
47
48
49
50
51
52
53
54
55
56
57
58
59
60

Introduction

1
2
3 33
4
5 34
6
7
8 35 A large radius secondary ion mass spectrometer (SIMS) has been used for stable isotope
9
10 36 analyses of geological samples at high precision and accuracy^{1,2}. Isotope analyses are performed
11
12 37 by sputtering of the sample surface using Cs⁺ or O⁻ primary ions that are focused, typically, to a
13
14 38 diameter of 10-15 μm; secondary ions ejected from the sample surface are extracted to the mass
15
16 39 spectrometer. Using the CAMECA IMS 1280 at the University of Wisconsin-Madison
17
18 40 (WiscSIMS Laboratory), we have developed high precision stable isotope analysis techniques
19
20 41 using primary beam sizes as small as 1-2 μm^{3,4}. However, positioning of the analysis location on
21
22 42 the sample surface using such a small primary beam was very difficult because the original
23
24 43 reflected light microscope of the IMS 1280 had an optical resolution of ~3.5 μm, which did not
25
26 44 allow the operator to see the 1-2 μm-size SIMS pits produced by sputtering of the sample surface
27
28 45 (Fig. 1a). As a consequence of this limitation, small-spot analyses at WiscSIMS were performed
29
30 46 as traverses of spots 2 or 3 μm apart by moving the sample in one direction (Fig. 1b) and the
31
32 47 exact locations were confirmed after SIMS analysis using scanning electron microscopy (SEM).
33
34 48 Even with a large analysis spot size of 10 μm, the low-resolution optical image leads to
35
36 49 positioning errors, such as analysis spots that overlap with an adjacent mineral phase or the
37
38 50 epoxy resin used for mounting grains, that result in inaccurate data. CAMECA IMS-series
39
40 51 instruments could be equipped with a secondary electron detector to image secondary electrons
41
42 52 produced from the sample surface by the sputtering of finely focused (<1 μm) Cs⁺ primary ions.
43
44 53 However, geological samples are often electrical insulators and require an electron-gun for
45
46 54 charge compensation that prevents use of a secondary electron detector. In addition, secondary
47
48 55 electron imaging does not work if the instrument is tuned with a positive secondary ion beam.
49
50
51
52
53
54
55
56
57
58
59
60

1
2
3 56 The resolution of the reflected light microscope of the first IMS 1280 instrument, which
4
5 57 was delivered to WiscSIMS in 2005, is determined by the geometry of the optical microscope,
6
7 58 the optical characteristics of its components, and the wavelength spectra of the white-light
8
9 59 source. It is difficult to modify the microscope geometry because of space constraints in the main
10
11 60 chamber that contains multiple high-voltage components. Alternatively, optical resolution would
12
13 61 be improved by using shorter wavelength and/or monochromatic light. Here, we report
14
15 62 modification of the optical microscope system of the IMS 1280 using a UV-light source. We
16
17 63 replaced multiple optical components to make them UV compatible, but did not make any
18
19 64 changes to the mechanical design of optics inside the vacuum chamber. In addition, we wrote a
20
21 65 LabVIEW-based software package for sample imaging.
22
23
24
25
26
27
28

29 67 **Modification of the optical microscope system**

30 68 **IMS 1280 reflected-light microscope system:**

31
32 69
33
34 70 The optical microscope system consists of three components: (1) an illuminator outside
35
36 71 of the vacuum chamber, (2) a reflected light microscope inside the vacuum, and (3) a zoom lens
37
38 72 and CCD camera outside of the vacuum (Fig. 2). The illuminator unit is placed outside of the
39
40 73 main chamber, which includes a halogen lamp for white light illumination, a condenser lens for
41
42 74 focusing light on the sample surface, and an adjustable angle mirror for illuminating the sample
43
44 75 surface with an incidence angle of 30° from normal. The optical microscope unit of the IMS
45
46 76 1280 is enclosed behind the extraction plate of the secondary ion optics, which is located 5mm
47
48 77 from the sample surface. The microscope unit consists of an optical waveguide enclosed within
49
50 78 the extraction plate, an objective lens, a mirror, and a transfer lens. The microscope is also
51
52
53
54
55
56
57
58
59
60

1
2
3 79 positioned 30° from normal to the sample surface opposite the angle of the illuminator. The
4
5 80 position of the objective lens along the optical axis is adjusted by manually rotating a knob that
6
7
8 81 is connected to the microscope unit via an UHV (ultra high vacuum) mechanical feedthrough.
9
10 82 There is a shutter placed in front of the waveguide to avoid deposits on the surface of waveguide
11
12 83 from material sputtered from sample. The field of view is 450 μm \times 380 μm at maximum
13
14 84 magnification of the zoom lens. Because of the angled view, the image is reduced in the Y-
15
16 85 direction relative to X to 87% (cosine of 30°) and shows defocusing in the Y direction on either
17
18 86 side of the center line. The originally supplied color CCD camera image with 752 (horizontal, H)
19
20 87 \times 582 (vertical, V) pixels was captured by the graphics board of the PC and displayed using
21
22 88 CAMECA software. One pixel of the image corresponded to 0.60 μm (H) \times 0.67 μm (V) on the
23
24 89 sample at maximum magnification, though effective resolution may be degraded by the factor of
25
26 90 two (\sim 1.2 μm) because of interpolating a color filter array (typically a unit of four pixels for red,
27
28 91 green, and blue) on the CCD.
29
30
31
32
33
34
35

93 **Blue LED light source:**

36
37
38 94 We first replaced the white-light source with a monochromatic blue ($\lambda\sim$ 455 nm) light
39
40 95 emitting diode (LED) without replacing any other optical components. We replaced the
41
42 96 illuminator assembly (designed by the Physical Science Laboratory, University of Wisconsin;
43
44 97 PSL) to adapt to a star configuration LED, which is described on the WiscSIMS website
45
46 98 (www.geology.wisc.edu/~wiscsims/). With this change to a shorter, monochromatic light, the
47
48 99 optical resolution was improved so that 3 μm lines of a resolution-calibration target were clearly
49
50 100 resolved (Fig. 3b), which could not be resolved in the original system (Fig. 3a). As a trade-off
51
52 101 with spatial resolution, this approach lost the color information of the sample surface. However,
53
54
55
56
57
58
59
60

1
2
3 102 color information is less important than the sharpness of the images because most of our
4
5 103 geological specimens are coated either by gold or carbon. Sample navigation is made by
6
7
8 104 identification of surface geometric features, such as cracks, pits, and differing surface textures,
9
10 105 that are compared to the detailed images taken from SEM or optical microscopes before the
11
12 106 samples were loaded into the SIMS.
13
14

15 107

17 108 **UV-light optics system:**

19
20 109 Subsequently, we modified the illumination to use a high power (700 mW) 365 nm UV
21
22 110 LED source. Several optical components that did not transmit UV were replaced with UV
23
24 111 compatible versions, including the optical waveguide, the objective lens, the mirror and the
25
26 112 transfer lens inside the vacuum chamber; as well as the condenser lens of the illuminator and the
27
28 113 zoom lens below the charge-coupled device (CCD) camera that are outside of the vacuum
29
30 114 chamber. The same illumination assembly was used as for the blue-LED-light source. The
31
32 115 original CCD camera was replaced with a UV-sensitive CCD camera capable of high definition
33
34 116 images (1380×1040 pixels). With this camera, one pixel of the image corresponds to 0.33 μm
35
36 117 (H) \times 0.38 μm (V) on the sample surface. These replacement components are listed in Table 1.
37
38 118 We note that the original mirror was a conventional back-surface mirror and transmitted UV-
39
40 119 light to a limited extent, but was replaced by a UV-compatible front-surface mirror. With the
41
42 120 original mirror, double reflections of the UV light were observed that disappeared after
43
44 121 replacement of the front-surface mirror. It seems that a small amount of light was reflected at the
45
46 122 non-coated front surface of the original mirror, which was enhanced when using the UV-light
47
48 123 due to its shorter wavelength. The double reflection images were displaced by a few μm
49
50 124 vertically, which degraded optical resolution significantly. As shown in Fig. 3c, the 2 μm lines of
51
52
53
54
55
56
57
58
59
60

1
2
3 125 the resolution-calibration target are now resolved and the 1.5 μm lines are resolved in the
4
5 126 horizontal direction.
6
7

8 127 LED light sources have higher requirements for heat dissipation, but at the same time
9
10 128 require less space than a conventional halogen lamp. The smaller space requirements allow a
11
12 129 further redesign of the illuminator optics. The redesign will improve the heat dissipation from
13
14 130 the LED while reducing the length and complexity of the optical path. This will improve the
15
16 131 efficiency of transmission of light from the LED into the vacuum chamber.
17
18
19

20 132

21
22 133 **Badgerscope© Sample Viewing Software:**
23

24 134 We wrote Badgerscope©, a new LabVIEW-based imaging software package, to
25
26 135 incorporate image manipulation because the new CCD camera is not compatible with the
27
28 136 CAMECA software and the PC interface provided with the instrument. The new software has
29
30 137 additional functionality compared to the original CAMECA software, which provides improved
31
32 138 accuracy and efficiency of targeting samples (see detail in ESI-1). Badgerscope© consists of an
33
34 139 image window to show CCD camera images with two targeting marks for analysis positions
35
36 140 (Fig. S1 in ESI-1). One of the marks is used as a reference point that is set at the beginning of
37
38 141 each analysis session to show the location of the primary beam. Another mark is used to navigate
39
40 142 sample stage positions (-10 mm to +10 mm in X and Y) by communicating with the CAMECA
41
42 143 software. It is possible to freely change the shape and position of these marks to accurately
43
44 144 reflect the actual beam. Badgerscope© allows improved signal/noise in images through variable
45
46 145 image averaging, enhanced images through manipulation of brightness and contrast and the use
47
48 146 of false color. It also has a “difference” function that displays the difference between a live
49
50 147 image and a reference image, allowing subtle changes to be detected, such as those made by a
51
52
53
54
55
56
57
58
59
60

1
2
3 148 short duration exposure of the primary beam to the sample surface (Fig. 4). This function is very
4
5 149 useful for small and low intensity primary beams, which sputter the sample surface very slowly
6
7
8 150 and leave pits that cannot otherwise be easily identified.
9

10 151

12 152 **Comparison between blue and UV-light illumination:**

13
14
15 153 The optical resolutions of blue-LED and UV-light optical systems are estimated using the
16
17 154 edge of a feature with a sharp boundary ($<0.1 \mu\text{m}$) on the resolution-calibration target (Fig. 3).
18
19 155 The estimated resolution, defined as the distance where the intensity changes by 50%, is $2.2 \mu\text{m}$
20
21 156 for the blue LED using the original optical system and $1.3 \mu\text{m}$ for the UV-light optical system.
22
23 157 These values are consistent with the resolution-calibration target images in Figs. 3b and c,
24
25 158 respectively. We compare two images of the resolution-calibration targets illuminated by the
26
27 159 blue LED and the UV-light LED using the same UV-light optical system (Fig. S2, ESI-2). Blue-
28
29 160 LED illumination on the new UV-light optical system resolved $2\text{-}\mu\text{m}$ lines, but not $1.5\text{-}\mu\text{m}$ lines
30
31 161 (Fig. S2, ESI-2), which indicates that the optical resolution is between $1.5 \mu\text{m}$ and $2 \mu\text{m}$. These
32
33 162 data indicate that the optical resolution is improved both by the replacement of the optical system
34
35 163 and the illumination source.
36
37
38
39

40
41 164 The maximum resolution (d) of an optical system is given by $d \sim 0.5\lambda/NA$, where λ and
42
43 165 NA are the wavelength of light and numerical aperture, respectively. Applying $NA = 0.12$ for the
44
45 166 IMS 1280 optical system, d is estimated to be $1.8 \mu\text{m}$ and $1.5 \mu\text{m}$, for blue-LED and UV-light
46
47 167 illumination, respectively. These values are comparable to the estimated optical resolution using
48
49 168 resolution-calibration targets. In addition to the improvements related to shorter wavelength,
50
51 169 there are other factors that improved the final resolution of the new system. The original color
52
53 170 camera operated at lower resolution with an effective pixel size corresponding to $\sim 1.2 \mu\text{m}$ on the
54
55
56
57
58
59
60

1
2
3 171 sample surface. The new higher resolution monochrome camera in the UV-light optical system
4
5 172 has an effective pixel size measuring 0.3-0.4 μm on the sample surface, so that the camera does
6
7
8 173 not limit the optical resolution. Replacement of the front-surface mirror resulted in clear and
9
10 174 sharp images without double reflections (Fig. S2, ESI-2). Although the geometric designs of
11
12 175 optical components are the same as in the original system, the replaced UV-grade optical
13
14 176 components may have higher optical quality, which may further reduce the various aberrations.
15
16
17
18 177

19
20 178 **Advantage of angled illumination:**

21
22 179 The angled illumination and camera view of the IMS 1280 optical system results in
23
24 180 defocusing of the sample image in the Y axis away from the center. This is a disadvantage in
25
26 181 viewing the sample image with the larger field of view of medium magnification ($\sim 800 \mu\text{m} \times$
27
28 182 $500 \mu\text{m}$), though it is not significant within the field of view at maximum magnification ($450 \mu\text{m}$
29
30 183 $\times 380 \mu\text{m}$). The defocusing effect along the Y direction is not changed with the new UV-light
31
32 184 optical system (Fig. S3, ESI-2). The angled view on the IMS 1280 has advantages in acquiring
33
34 185 reliable stable isotope measurements. Topography of the sample surface may degrade accuracy
35
36 186 of stable isotope analyses because a tilted surface deforms the surface potential ($\pm 10\text{kV}$) where
37
38 187 secondary ions are ejected. Kita et al.² recommended that surface topography of samples should
39
40 188 be less than $3 \mu\text{m}$ in order to obtain accurate results. Although we inspect the topography of each
41
42 189 sample mount prior to SIMS analysis, edges of grains sometimes show small amounts of
43
44 190 topography. The angled illumination of the IMS 1280 optical system is very sensitive to surface
45
46 191 topography compared to normal-incidence illumination. The heterogeneous brightness of the
47
48 192 sample surface would indicate surface topography is significant. We can determine the beam
49
50
51
52
53
54
55
56
57
58
59
60

1
2
3 193 position on the sample for reliable analysis guided by reflected-light illumination with the
4
5
6 194 improved optical resolution.
7

8 195

10 196 **Application of the new UV-light microscope system to SIMS analysis**

12 197

15 198 **Alignment of the primary beam:**

17 199 One of the important aspects of SIMS analysis is tuning the primary beam for intensity
18
19
20 200 and size that is optimized for a research goal. The primary-beam size is typically 10-15 μm for
21
22 201 stable isotope analysis, but should be small enough that the beam does not overlap multiple
23
24 202 phases. Overlap of the beam with different minerals would result in a mixed analysis and
25
26
27 203 erroneous instrumental bias corrections. Even within a single mineral grain, geological
28
29 204 specimens are often zoned in chemistry and isotope ratios that correspond to distinct events or
30
31
32 205 environments in geologic time and space, so that primary beam size should ideally be smaller
33
34 206 than the dimensions of the zoning. However, the primary beam current commonly decreases with
35
36 207 approximately the square of beam diameter, which results in poorer precision of isotope ratio
37
38 208 measurements due to lower secondary ion intensities. Therefore, the analyst must optimize
39
40
41 209 intensity and beam-spot size for each analysis session in order to maximize the scientific value of
42
43 210 the analysis. The distribution of primary beam intensities within a given primary beam spot is
44
45
46 211 also important. In the case of oxygen isotope ratio measurements of Ca carbonate,
47
48 212 reproducibility of the calcite standard degraded if the primary beam is better focused (Gaussian
49
50 213 beam) and makes a deeper sputter crater. Rastering the primary beam during the analysis would
51
52
53 214 produce flatter crater shape, though it would enlarge the size of analysis spot.
54
55
56
57
58
59
60

1
2
3 215 Primary beam alignment is generally performed by illuminating secondary ions from a
4
5
6 216 homogeneous material (such as a Si-wafer) using direct ion imaging. The secondary ions are
7
8 217 projected onto the multi-channel plate (MCP) at the end of the secondary ion path, showing the
9
10 218 size, shape, and density distribution of the primary beam. However, the lateral resolution of the
11
12 219 direct ion image is relatively poor (~a few μm) when apertures and slits of the mass spectrometer
13
14 220 are fully opened to achieve high secondary ion transmission (~90%). The new UV-light optics
15
16 221 allow us to evaluate the size and density distribution of the primary beam more easily by
17
18 222 optically imaging craters sputtered in a clean Si wafer (Fig. 5a). The Badgerscope© software
19
20 223 makes various kinds of false color images (Fig. 5b), which can be used to vary the contrast
21
22 224 differences so as to enhance observation of the heterogeneity of primary beam density within a
23
24 225 primary beam spot.
25
26
27
28
29
30

226

227 **Application to paleoclimate research:**

31
32
33
34 228 Fig. 6 shows an example of SIMS analysis of a planktic foraminifera that employs
35
36 229 oxygen isotope ratios to distinguish the primary foraminifera calcite shell from secondary
37
38 230 diagenetic crystallites⁶. Conventional stable isotope analysis of whole shells of foraminifera
39
40 231 would produce erroneous results due to contamination by diagenetic calcite. Prior to SIMS
41
42 232 analysis, secondary electron (SE) imaging of the sample was conducted so as to assist navigation
43
44 233 between analysis positions. The SE images show surface features, such as cracks and
45
46 234 topography, consistent with the reflected light image. True paleoclimate signatures are preserved
47
48 235 only in the thin chamber wall ($\leq 10 \mu\text{m}$ thickness), which can be analyzed using 3- μm SIMS
49
50 236 spots. The new UV light microscope shows clearly the location of the thin chamber wall so that
51
52
53 237 the analyst can precisely separate the chamber wall and diagenetic cement for analysis. The
54
55
56
57
58
59
60

1
2
3 238 results of SIMS analysis have been used to confirm a global temperature rise at the Paleocene-
4
5 239 Eocene boundary⁶ (55.8 million years ago).
6
7
8 240

9
10 241 **Beyond optical resolution:**
11

12 242 The analysis of samples using a beam size of $2\ \mu\text{m} \times 1\ \mu\text{m}$ is much easier with UV-light
13
14 243 than white light illumination because it is possible to see the SIMS pits during analysis. These
15
16 244 small pits were not visible with the original viewing system. However, accurate positioning of
17
18 245 the beam requires care because the beam size and the optical resolution are comparable.
19
20 246 Nakashima et al.⁷ developed a new targeting procedure that combines Focused Ion Beam (FIB)
21
22 247 milling to delicately remove the surface coating of a $1\ \mu\text{m} \times 1\ \mu\text{m}$ target area, which can then be
23
24 248 viewed using SIMS secondary ion imaging with a scanning sub- μm primary beam (Fig. 7). The
25
26 249 new UV-light optics with improved optical resolution were necessary for locating the specimen
27
28 250 for secondary ion imaging (Fig. 7b). Using this technique, it is possible to aim and hit small
29
30 251 specimens with a reproducibility of $0.5\ \mu\text{m}$. As a result, Nakashima et al.⁷ analyzed the center of
31
32 252 comet particles as small as $2\ \mu\text{m} \times 4\ \mu\text{m}$, which could not be done previously during a study by
33
34 253 Nakamura et al.⁴. The accurate targeting of small particles is important for precious space-
35
36 254 mission return-particle analyses, such as the Stardust Mission where a majority of the particles
37
38 255 collected are much smaller than $10\ \mu\text{m}$ ⁸.
39
40
41
42
43
44
45
46
47

48 257 **Summary**
49
50
51 258

52
53 259 We have modified the reflected-light microscope system of a CAMECA IMS 1280 SIMS
54
55 260 using UV-light and compatible optical components. These changes improved spatial resolution
56
57
58
59
60

1
2
3 261 when viewing samples from $\sim 3.5 \mu\text{m}$ to $\sim 1.3 \mu\text{m}$. The new Badgerscope© software improved
4
5 262 our positioning accuracy and efficiency, which contributes greatly to the quality of SIMS
6
7
8 263 analyses. Using the secondary ion imaging technique, we achieved positioning accuracy as good
9
10 264 as $0.5 \mu\text{m}$. A similar modification using a UV-light source would be applicable to the optical
11
12 265 microscope system of other instruments such as an electron microprobe when there are
13
14
15 266 limitations of mechanical re-design, but need for better imaging resolution.
16
17
18 267

19
20 268 **Acknowledgements:** This work is supported by the NSF-EAR Instrumentation and Facilities
21
22 269 Program (EAR-0744079, -1053466, -1355590). Part of the engineering design and the
23
24 270 determination of optical properties of the original microscope optical components were made by
25
26
27 271 Ken Kriesel and Dan Wahl under contract with the Physical Sciences Laboratory, University of
28
29 272 Wisconsin. We thank John Craven (Edinburgh University) for loan of CAMECA 4f optical
30
31 273 components, and Emmanuel De Chambost, Fabrice Le Duigou, and Paula Peres (CAMECA
32
33 274 Instruments) for technical assistance and advice. Reinhard Kozdon kindly provided the image of
34
35 275 a foraminifera sample by UV-light microscope. Constructive comments by anonymous referees
36
37
38 276 improved the clarity of the manuscript. We also thank to Daisuke Nakashima, Takayuki
39
40 277 Ushikubo, Kouki Kitajima, and colleagues in the WiscSIMS laboratory for helpful suggestions
41
42
43 278 and assistance for the project.
44
45

46 279
47
48
49
50
51
52
53
54
55
56
57
58
59
60

References

- 1
2
3 280
4
5
6 281
7
8 282 1. J. W. Valley and N. T. Kita, *Mineralogical Association of Canada Short Course*, 2009, **41**, 19-
9
10 283 63.
11
12 284 2. N. T. Kita, T. Ushikubo, B. Fu and J. W. Valley, *Chem. Geol.*, 2009, **264**, 43-57.
13
14 285 3. F. Z. Page, T. Ushikubo, N. T. Kita, L. R. Riciputi and J. W. Valley, *Am. Mineral.*, 2007, **92**,
15 286 1772-1775.
16
17 287 4. T. Nakamura, T. Noguchi, A. Tsuchiyama, T. Ushikubo, N. T. Kita, J. W. Valley, M. E.
18 288 Zolensky, Y. Kakazu, K. Sakamoto, E. Mashio, K. Uesugi and T. Nakano *Science*, 2008,
19 289 **321**, 1664-1667.
20
21 290 5. N. T. Kita, T. Ushikubo, K. B. Knight, R. A. Mendybaev, A. M. Davis, F. M. Richter and J. H.
22 291 Fournelle, *Geochim. Cosmochim. Acta*, 2012, **86**, 37-51.
23
24 292 6. R. Kozdon, D. C. Kelly, K. Kitajima, A. Strickland, J. H. Fournelle and J. W. Valley
25 293 *Paleoceanography*, 2013, **28**, 517-528.
26
27 294 7. D. Nakashima, T. Ushikubo, D. J. Joswiak, D. E. Brownlee, G. Matrajt, M. K. Weisberg, M.
28 295 E. Zolensky and N. T. Kita, *Earth Planet. Sci. Lett.*, 2012, **357-358**, 355-365.
29
30 296 8. D. E. Brownlee, D. J. Joswiak and G. Matrajt, *Meteorit. Planet. Sci.*, 2012, **47**, 453-470.
31
32
33
34
35
36
37
38
39
40
41
42
43
44 297
45
46
47
48
49
50
51
52
53
54
55
56
57
58
59
60

298 Table 1. List of components replaced for the UV light optical system.

Components	Part numbers or material used
Light source	LED Engin LZ1-10U600
Illuminator condenser lens	CAMECA 91480823
Waveguide	UV grade fused silica rod Tower Optical 4520-0162
Objective lens assembly	CAMECA 91480827
Mirror	Edmonds Optics 68-316
Transfer lens assembly	CAMECA 91480826
Zoom lens	Pentax B2528-UV lens
HD Camera	JAI CM-140GE-UV

299

300

Figure Captions

1
2
3 301
4
5 302
6
7
8 303 Fig. 1. An example of the images obtained with the original reflected microscope of a CAMECA
9
10 304 IMS 1280 for a particle from the Wild 2/81P comet sampled by the NASA Stardust Mission. (a)
11
12 305 Reflected light microscope image of the particle “Gozen-sama” (C2081,1,108,1) during SIMS
13
14 306 analysis in 2007. The enlarged view of the dotted square is shown in the insert at the right-top
15
16 307 corner, which includes the particle that is outlined by a dashed line. The blue dot in the center
17
18 308 indicates the position of SIMS analyses. (b) High resolution back-scattered electron image of the
19
20 309 same particle after the SIMS analyses (Nakamura et al. ⁴). Analyses were made as two traverses
21
22 310 of 2 μm spots (numbered 1-10) and a 6 \times 6 grid of 1- μm spots. Filled red and white dots
23
24 311 correspond to the locations of 2 μm and 1 μm spot analyses, respectively, that show a large
25
26 312 mass-independent isotope anomaly in ¹⁶O. During the grid analysis, backlash of the sample stage
27
28 313 stepping motors resulted significant overlap between the first and second traverses (right end), as
29
30 314 well as the first and second spots of every traverse (i.e., 6 spots look like only 5 spots). Fig. 1b is
31
32 315 rotated CW relative to 1a; the yellow arrows indicate the orientation of the particle.
33
34 316
35
36
37
38
39
40

41 317 Fig. 2. Schematic diagram of the reflected light microscope system of a CAMECA IMS 1280.
42
43 318 Names in the boxes are parts that were replaced for the UV-light optical system. Illumination
44
45 319 light source, zoom lens, and camera are located outside of the vacuum chamber. Illuminator unit
46
47 320 is not shown in detail. See main text for a detailed description.
48
49
50
51
52

53 322 Fig. 3. Reflected-light microscope images of a resolution-calibration target, CAMECA SIMS test
54
55 323 sample. Numbers next to each set of lines (1.0 to 5) indicate width and distance between lines in
56
57
58
59
60

1
2
3 324 micro-meters. Resolution of an image corresponds to the minimum width of lines that can be
4
5 325 resolved. (a) Original CAMECA IMS 1280 microscope image with white light source.
6
7
8 326 Resolution $\sim 3.5 \mu\text{m}$. Full color image. (b) Modification to blue LED light source (455 nm).
9
10 327 Resolution $\sim 2.2 \mu\text{m}$. Blue color image. (c) UV light system using LED-light source (365 nm).
11
12 328 Resolution $\sim 1.3 \mu\text{m}$. Monochrome image.
13
14
15 329
16
17 330
18
19

20 331 Fig. 4. Example of the “difference function” in the Badgerscope© software. Four images are
21
22 332 shown on the slightly pitted surface of a Si-wafer. (a) Normal microscope image of sample
23
24 333 surface before sputtering, showing numerous dots and shadows in similar size and brightness to
25
26 334 small SIMS spots. Brightness and contrast are optimized. Blue oval is a marker to navigate
27
28 335 sample stage motions. (b) Normal microscope image after sputtering with a small SIMS spot (~ 2
29
30 336 $\mu\text{m Cs}^+$ beam). The position of SIMS spot is identified (inside blue oval) by comparing images
31
32 337 (a) and (b). (c) Image using the difference function before sputtering starts. The image shows
33
34 338 only a black background because the live-image does not change from the original image in (a).
35
36 339 (d) Image using the difference function during sputtering. A bright spot appears within a few
37
38 340 seconds at the location where the primary beam hits the sample due to subtle changes of
39
40 341 brightness.
41
42
43
44
45
46 342
47

48 343 Fig. 5. The UV-light microscope images of primary beam spots on a clean Si-wafer. The
49
50 344 example shows primary beam spots with various sizes and shapes when O^- primary ions were
51
52 345 aligned for Köhler illumination conditions⁵. (a) Normal grey scale image with optimized
53
54 346 brightness and contrast. (b) False-color image, which shows surface topography of sputtered
55
56
57
58
59
60

1
2
3 347 craters. Sizes and shapes of individual spots differ due to changes in aperture size and parameters
4
5 348 of the primary ion column, which are examined by observing spots on a Si-wafer using the UV-
6
7
8 349 light microscope. The primary beam parameters are chosen to optimize the primary beam
9
10 350 conditions.

11
12 351
13
14
15 352 Fig. 6. Oxygen isotope analyses of a foraminifera and diagenetic cement from an Ocean Drilling
16
17 353 Program core sample (Kozdon et al.⁶). (a) Scanning electron (SE) image of the shell of a
18
19 354 planktonic foraminifer before mounting in epoxy resin. (b) The UV-light microscope image of
20
21 355 the cross section after SIMS analysis (Field of view ~150 μm). Two parallel traverses of 10 μm
22
23 356 and 3 μm SIMS spots are shown. (c) SE image of the same cross section after 3 μm spot
24
25 357 analyses. Thin chamber walls of the foraminifer (spot numbers 1-5) were accurately aimed using
26
27 358 the UV-light microscope. (d) Oxygen isotope analyses of the foraminifer and cement with 3- μm
28
29 359 spots. Paleoclimate isotope signatures are only recorded in the thin chamber wall and could not
30
31 360 be studied without a small beam spot. Accurate aiming of these spots required UV illumination.
32
33 361

34
35
36 362 Fig. 7. FIB marking technique for aiming of a SIMS analysis target at sub- μm accuracy
37
38
39 363 (Nakashima et al.⁷). (a) SEM image of the Wild 2 particle (Track 77 fragment 4; 4 $\mu\text{m} \times 4 \mu\text{m}$)
40
41 364 with 1 μm square FIB mark where surface carbon coating was removed. The particle has a nm-
42
43 365 scale irregular surface from microtome slicing during sample preparation. (b) The scanning ion
44
45 366 image ($^{16}\text{O}^-$) of the particle before oxygen isotope analysis using finely focused ($\leq 1 \mu\text{m}$) primary
46
47 367 beam across a 10 $\mu\text{m} \times 10 \mu\text{m}$ area, showing the FIB mark with high secondary O^- signals. (c)
48
49 368 The scanning ion image of the particle after SIMS analysis using a 2 $\mu\text{m} \times 1 \mu\text{m}$ spot. (d) SEM
50
51 369 image of the particle with SIMS spot at the center.
52
53
54
55
56
57
58
59
60

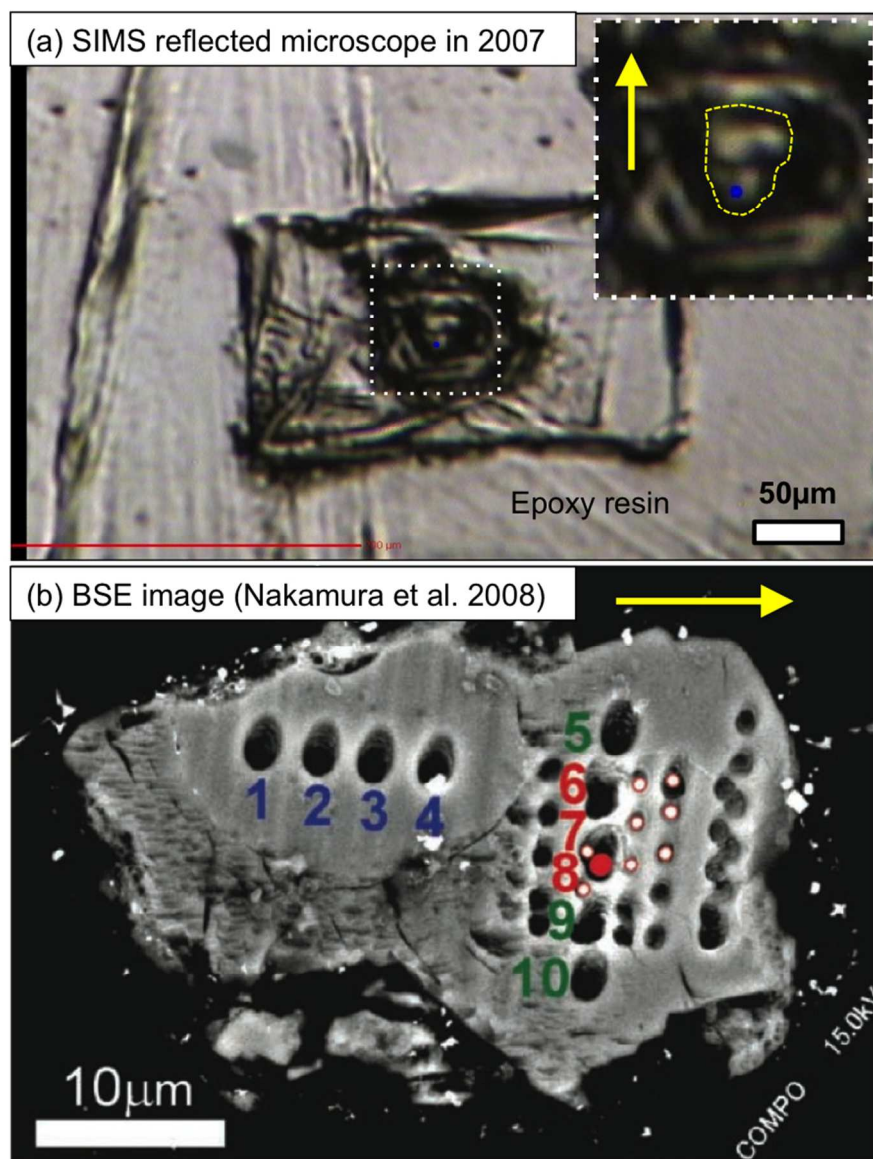


Fig. 1. An example of the images obtained with the original reflected microscope of a CAMECA IMS 1280 for a particle from the Wild 2/81P comet sampled by the NASA Stardust Mission. (a) Reflected light microscope image of the particle "Gozen-sama" (C2081,1,108,1) during SIMS analysis in 2007. The enlarged view of the dotted square is shown in the insert at the right-top corner, which includes the particle that is outlined by a dashed line. The blue dot in the center indicates the position of SIMS analyses. (b) High resolution back-scattered electron image of the same particle after the SIMS analyses (Nakamura et al. ⁴). Analyses were made as two traverses of 2-µm spots (numbered 1-10) and a 6×6 grid of 1-µm spots. Filled red and white dots correspond to the locations of 2-µm and 1-µm spot analyses, respectively, that show a large mass-independent isotope anomaly in ¹⁶O. For the grid analysis, backlash of the sample stage stepping motors resulted significant overlap between the first and second traverses (right end), as well as the first and second spots of every traverse (i.e., 6 spots look like only 5 spots). Fig. 1b is rotated CW relative to 1a; the yellow arrows indicate the orientation of the particle.

327x431mm (72 x 72 DPI)

1
2
3
4
5
6
7
8
9
10
11
12
13
14
15
16
17
18
19
20
21
22
23
24
25
26
27
28
29
30
31
32
33
34
35
36
37
38
39
40
41
42
43
44
45
46
47
48
49
50
51
52
53
54
55
56
57
58
59
60

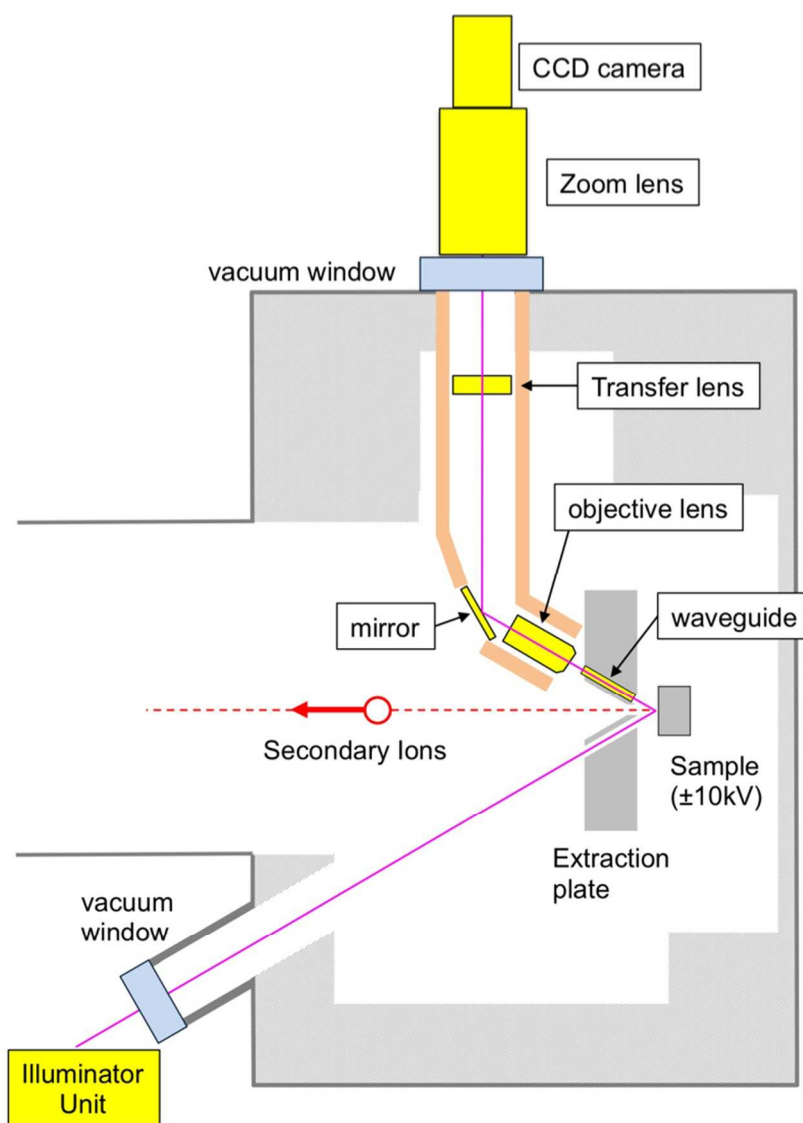


Fig. 2. Schematic diagram of the reflected light microscope system of a CAMECA IMS 1280. Names in the boxes are parts that were replaced for the UV-light optical system. Illumination light source, zoom lens, and camera are located outside of the vacuum chamber. Illuminator unit is not shown in detail. See main text for a detailed description.

308x415mm (72 x 72 DPI)

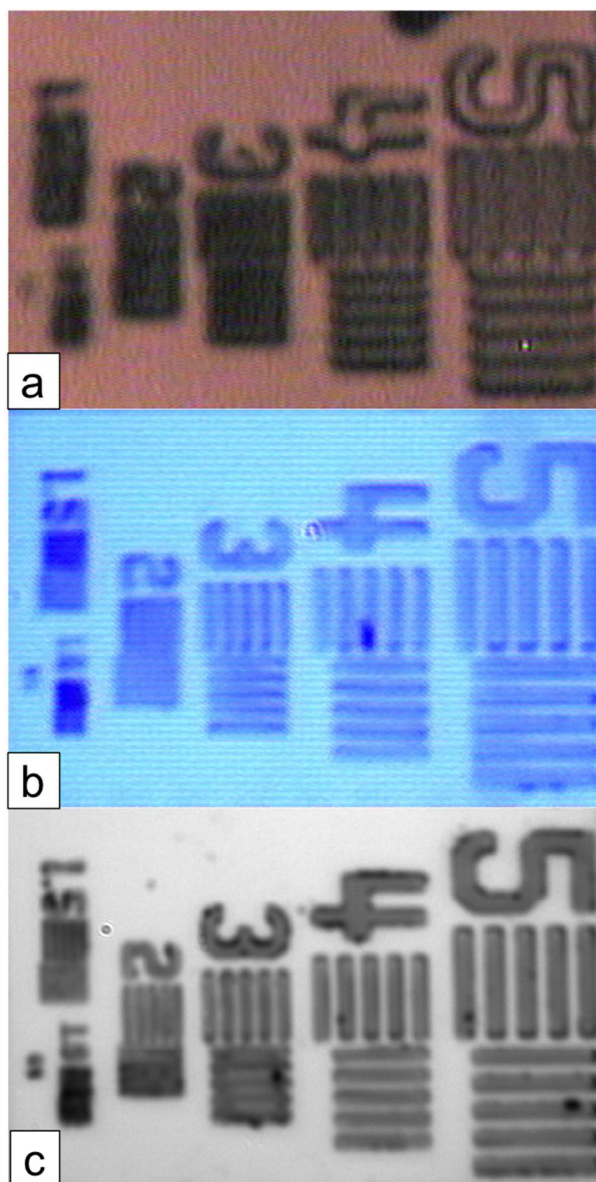


Fig. 3. Reflected-light microscope images of a resolution-calibration target, CAMECA SIMS test sample. Numbers next to each set of lines (1.0 to 5) indicate width and distance between lines in micrometers. Resolution of an image corresponds to the minimum width of lines that can be resolved. (a) Original CAMECA IMS 1280 microscope image with white light source. Resolution $\sim 3.5 \mu\text{m}$. Full color image. (b) Modification to blue LED light source (455 nm). Resolution $\sim 2.2 \mu\text{m}$. Blue color image. (c) UV light system using LED-light source (365 nm). Resolution $\sim 1.3 \mu\text{m}$. Monochrome image. 240x459mm (72 x 72 DPI)

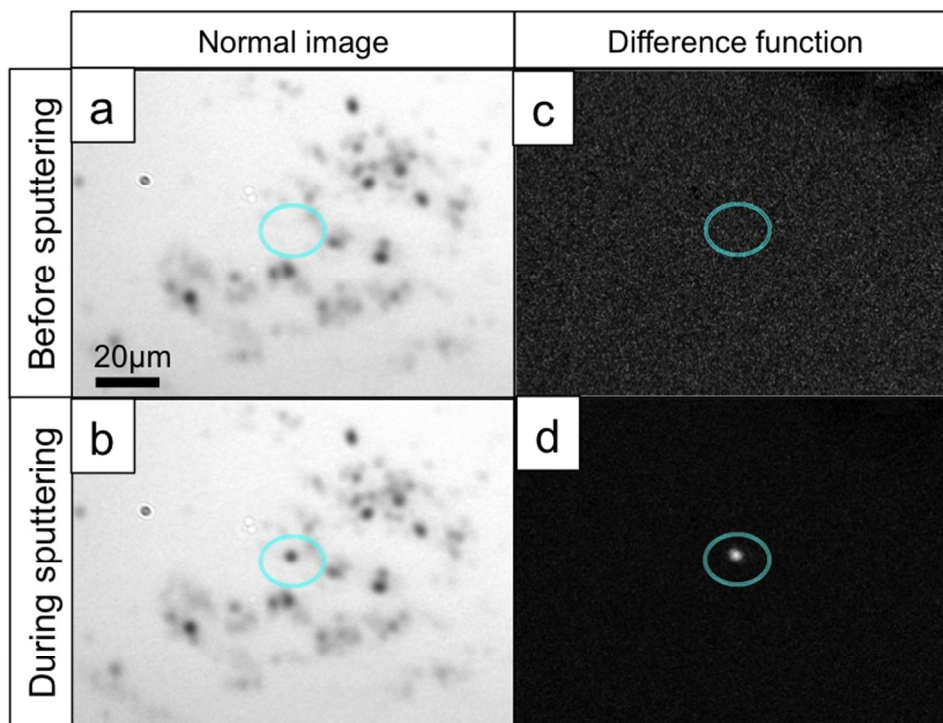


Fig. 4. Example of the “difference function” in the Badgerscope© software. Four images are shown on the slightly pitted surface of a Si-wafer. (a) Normal microscope image of sample surface before sputtering, showing numerous dots and shadows in similar size and brightness to small SIMS spots. Brightness and contrast are optimized. Blue oval is a marker to navigate sample stage motions. (b) Normal microscope image after sputtering with a small SIMS spot ($\sim 2 \mu\text{m}$ Cs^+ beam). The position of SIMS spot is identified (inside blue oval) by comparing images (a) and (b). (c) Image using the difference function before sputtering starts. The image shows only a black background because the live-image does not change from the original image in (a). (d) Image using the difference function during sputtering. A bright spot appears within a few seconds at the location where the primary beam hits the sample due to subtle changes of brightness.

305x230mm (72 x 72 DPI)

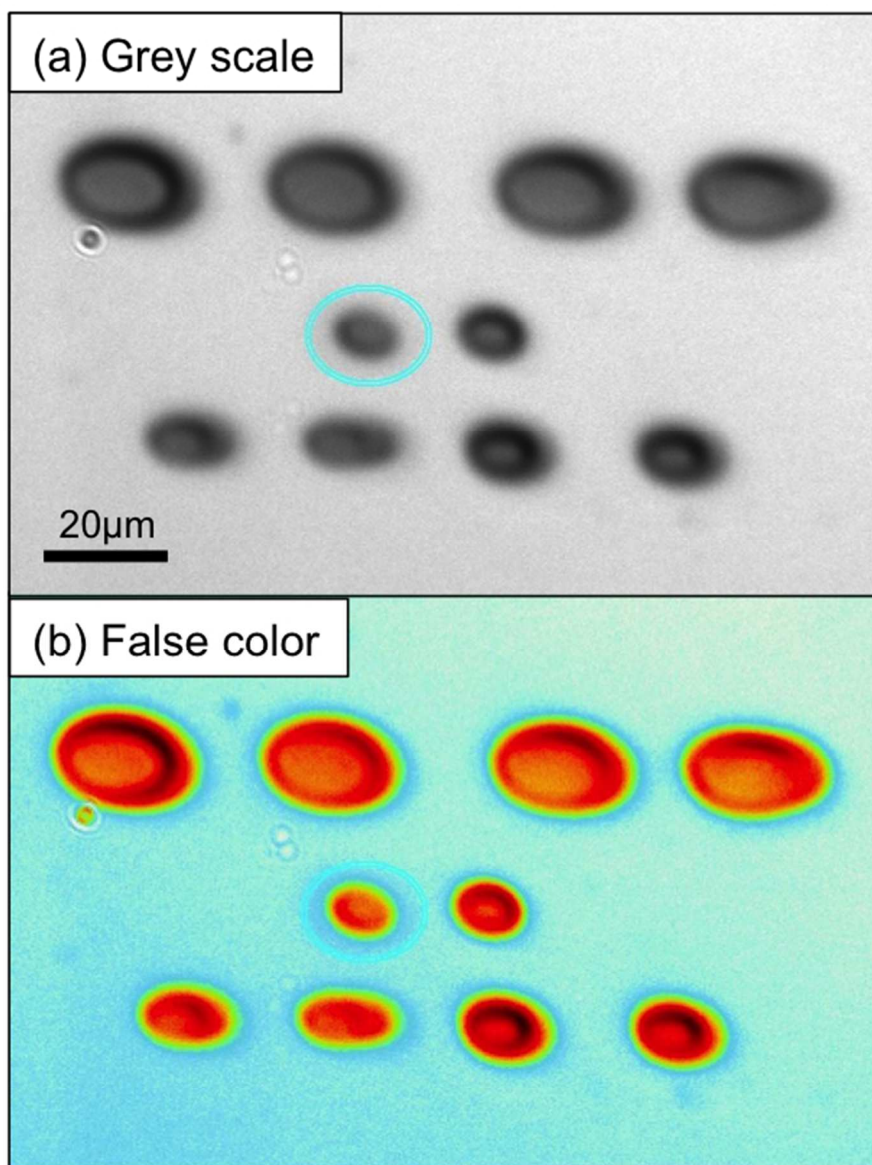


Fig. 5. The UV-light microscope images of primary beam spots on a clean Si-wafer. The example shows primary beam spots with various sizes and shapes when O⁻ primary ions were aligned for Köhler illumination conditions⁵. (a) Normal grey scale image with optimized brightness and contrast. (b) False-color image, which shows surface topography of sputtered craters. Sizes and shapes of individual spots differ due to changes in aperture size and parameters of the primary ion column, which are examined by observing spots on a Si-wafer using the UV-light microscope. The primary beam parameters are chosen to optimize the primary beam conditions.
223x293mm (72 x 72 DPI)

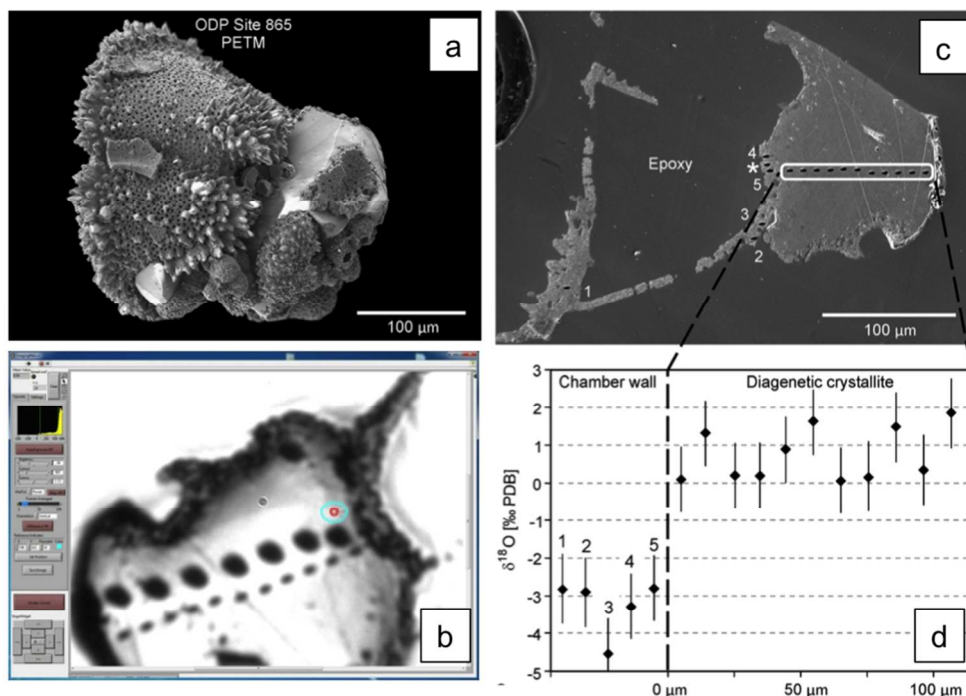


Fig. 6. Oxygen isotope analyses of a foraminifera and diagenetic cement from an Ocean Drilling Program core sample (Kozdon et al.⁶). (a) Scanning electron (SE) image of the shell of a planktonic foraminifer before mounting in epoxy resin. (b) The UV-light microscope image of the cross section after SIMS analysis (Field of view ~150 μm). Two parallel traverses of 10 μm and 3 μm SIMS spots are shown. (c) SE image of the same cross section after 3 μm spot analyses. Thin chamber walls of the foraminifer (spot numbers 1-5) were accurately aimed using the UV-light microscope. (d) Oxygen isotope analyses of the foraminifer and cement with 3-μm spots. Paleoclimate isotope signatures are only recorded in the thin chamber wall and could not be studied without a small beam spot. Accurate aiming of these spots required UV illumination.

355x253mm (72 x 72 DPI)

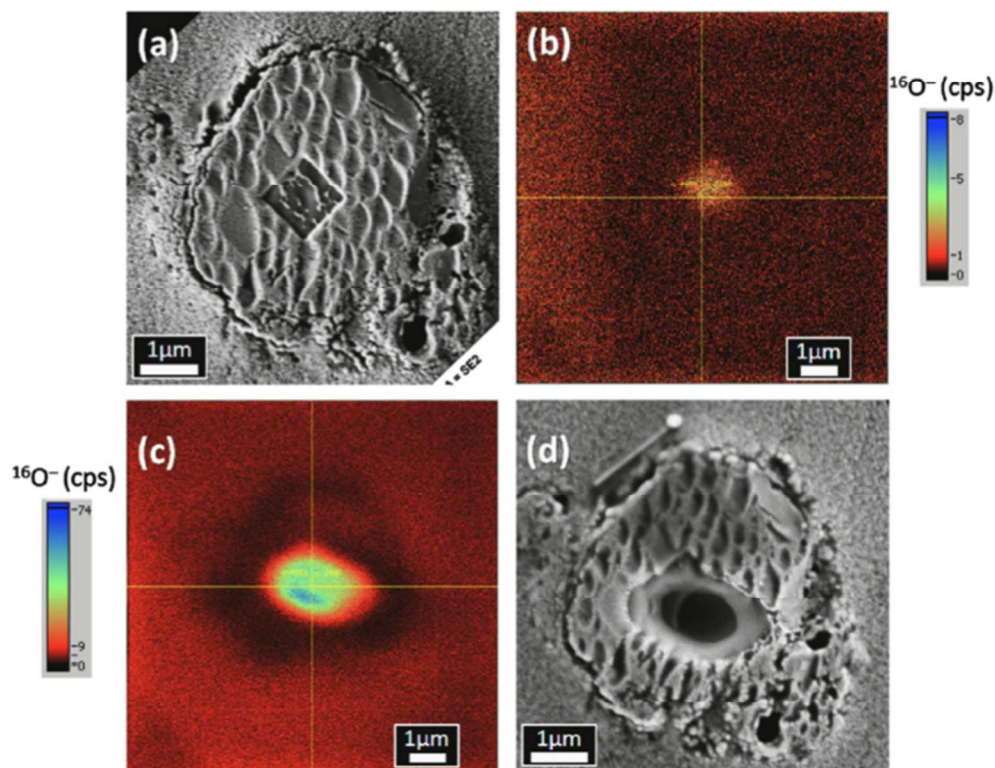


Fig. 7. FIB marking technique for aiming of a SIMS analysis target at sub- μm accuracy (Nakashima et al.⁷). (a) SEM image of the Wild 2 particle (Track 77 fragment 4; $4 \mu\text{m} \times 4 \mu\text{m}$) with $1 \mu\text{m}$ square FIB mark where surface carbon coating was removed. The particle has a nm-scale irregular surface from microtome slicing during sample preparation. (b) The scanning ion image ($^{16}\text{O}^-$) of the particle before oxygen isotope analysis using finely focused ($\leq 1 \mu\text{m}$) primary beam across a $10 \mu\text{m} \times 10 \mu\text{m}$ area, showing the FIB mark with high secondary O^- signals. (c) The scanning ion image of the particle after SIMS analysis using a $2 \mu\text{m} \times 1 \mu\text{m}$ spot. (d) SEM image of the particle with SIMS spot at the center.
299x248mm (72 x 72 DPI)